Exciton Dynamics in the Chlorosomal Antennae of the Green Bacteria *Chloroflexus aurantiacus* and *Chlorobium tepidum*

V. I. Prokhorenko, D. B. Steensgaard, and A. R. Holzwarth
Max-Planck-Institut für Strahlenchemie, D-45413, Mülheim a.d. Ruhr, Germany

ABSTRACT The energy transfer processes in isolated chlorosomes from green bacteria *Chlorobium tepidum* and *Chloroflexus aurantiacus* have been studied at low temperatures (1.27 K) by two-pulse photon echo and one-color transient absorption techniques with ~100 fs resolution. The decay of the coherence in both types of chlorosomes is characterized by four different dephasing times stretching from ~100 fs up to 300 ps. The fastest component reflects dephasing that is due to interaction of bacteriochlorophylls with the phonon bath, whereas the other components correspond to dephasing due to different energy transfer processes such as distribution of excitation along the rod-like aggregates, energy exchange between different rods in the chlorosome, and energy transfer to the base plate. As a basis for the interpretation of the excitation dephasing and energy transfer pathways, a superlattice-like structural model is proposed based on recent experimental data and computer modeling of the Bchl *c* aggregates (1994. *Photosynth. Res.* 41:225–233.) This model predicts a fine structure of the Q_y absorption band that is fully supported by the present photon echo data.

INTRODUCTION

In green bacteria the chlorosomes form the major light-harvesting antenna (Olson, 1998). They contain a large number of special bacteriochlorophylls (BChls, up to several tens of thousands) that are assembled in rod-like aggregates (Staehelin et al., 1978, 1980). In chlorosomes from both the green gliding bacterium *Chloroflexus aurantiacus* and the green sulfur bacterium *Chlorobium tepidum*, the main pigment (≈99%) is BChl *c*. The rod-like BChl *c* aggregates, which do not seem to contain proteins (Griebenow and Holzwarth, 1989; Hirota et al., 1992), are tightly packed and surrounded by a lipid-like sack, and they form a hexagonal matrix (Staehelin et al., 1978, 1980). The former can be considered as a two-dimensional superlattice structure, which contains between 10 and 30 rod-like aggregates. Light energy, absorbed by these BChl aggregates, is efficiently transferred to the BChl *a* containing base plate, connected to the chlorosomal vesicle, and further to the reaction centers, where the primary photosynthetic reaction occurs.

The energy transfer processes within the chlorosomal Bchl aggregates and from the aggregates to the base plate have been intensively studied in recent years by means of femto- and picosecond transient absorption spectroscopy (TA), time-resolved fluorescence, and hole-burning spectroscopy (HB). Using one- and two-color TA with femtosecond resolution on chlorosomes of *Cf. aurantiacus* at room temperature, energy transfer lifetimes of 50–100 fs, 1–2 ps, and 7–10 ps were found (Savikhin et al., 1994). The longest component was assigned to the energy transfer between rod aggregates. However, in earlier papers (Griebenow et al., 1990; Müller et al., 1990, 1993) it was convincingly shown by means of time-resolved fluorescence that this component characterized energy transfer from the chlorosomal aggregates to the base plate. Similar lifetimes were reported from one-color measurements in the same type of chlorosomes at 77 K (Ma et al., 1996a), i.e., 50–60 fs, 1–2 ps, 7–20 ps, and a very long-lived component of 90–150 ps. In this study, the dispersive behavior of the lifetimes was pointed out. By means of two-color TA in *Cf. aurantiacus* chlorosomes at 19 K, the rise time of ~300 fs in the 731–750 nm absorption difference time profiles was assigned to an energy transfer among different spectral forms of BChl *c* (Savikhin et al., 1996a). However, at room temperatures such subpicosecond downhill energy transfer was not observed (Savikhin et al., 1996b). Energy transfer in chlorosomes of *Cb. tepidum* has been also studied with femtosecond resolution at room temperatures (Savikhin et al., 1995a; two-color TA of isolated chlorosomes) and at 5–65 K (Psencik et al., 1998; one-color TA of whole cells). At low temperatures the initial bleaching in the Q_y absorption band of the chlorosomes decayed with lifetimes of 200–300 fs, 1.7–1.8 ps, 5.4–5.9 ps, 30–40 ps and a long-lived ~300 ps component. This was in contrast to room temperature, where the decays showed only a 1–2 ps and ~30 ps component. It is also important that in all TA experiments the fast damped oscillations have been observed in the absorption difference signals with frequencies of ~50 cm^{-1} and 100–250 cm^{-1} in *Cf. aurantiacus* (Savikhin et al., 1994), and 70–80 cm^{-1}, and 130–140 cm^{-1} in *Cb. tepidum* chlorosomes (Savikhin et al., 1995a), respectively. (In another paper (Savikhin et al., 1995b), oscillations with frequencies of ~30, 90, and 130 cm^{-1} were reported.) The origin of these oscillations is not quite clear. In the work of Savikhin et al. (1994) two possible explana-

Received for publication 18 January 2000 and in final form 17 July 2000.
A preliminary account of this work was given at the IVth Workshop on Green and Heliobacteria, Girona, Spain, August, 1999.
Address reprint requests to Prof. A. R. Holzwarth, Max-Planck-Institut für Strahlenchemie, D-45413, Mülheim a.d. Ruhr, Germany. Tel.: 49-208-306-3571; Fax: 49-208-306-3951; E-mail: holzwarth@mpi-muelheim.mpg.de.

0006-3495/00/10/2105/16 $2.00

tions have been discussed: an electronic beating arising from interference between closely spaced exciton states, and a manifestation of intramolecular vibrational levels (vibrational wavepacked coherence).

Energy transfer within the chlorosomes from both green sulfur bacteria (Causgrove et al., 1990; van Walree et al., 1999) and green filamentous bacteria (Griebenow et al., 1990; Müller et al., 1990, 1993; Causgrove et al., 1990; Ma et al., 1996b) has been studied by means of time-resolved fluorescence spectroscopy. Under reducing conditions the chlorosomes are strongly fluorescent, with main lifetime components in the range of 30–80 ps. Recently, chlorosomes of *Cb. limicola* containing 50% BChl *d* and BChl *c* each were studied, and energy transfer between these two pools of BChl aggregates had a time constant of ~4 ps at 80 K (Steensgaard et al., 2000). This number gives some clue as to the rate of energy transfer between different rods in the chlorosomal aggregate.

The HB investigations on chlorosomes from different types of bacteria show that the lowest exciton state in the Q_y absorption region of Bchl *c* and *d* aggregates is inhomogeneously broadened (FWHM ~ 90–100 cm^{-1}) and from the zero-photon hole analysis the excited state lifetimes T_1 of ~10 ps for the *Chloroflexus aurantiacus* (Fetisova and Mauring, 1992), 5–10 ps for the *Chlorobium limicola* (Fetisova and Mauring, 1993; Psencik et al., 1994), and ~6 ps for the *Chlorobium tepidum* bacteria (Psencik et al., 1998) were reported.

On the basis of a large number of spectroscopic data (Holzwarth et al., 1990a, 1992; Hildebrandt et al., 1991, 1994; Holzwarth and Schaffner, 1994; Chiefari et al., 1995; Tamiaki et al., 1996; Balaban et al., 1997) we had previously developed an organizational model for the self-aggregated structures present in chlorosomes by molecular modeling procedures (Holzwarth and Schaffner, 1994; Schaffner and Holzwarth, 1997). The validity of this model has been tested and confirmed more recently by both solid state NMR (Balaban et al., 1995; van Rossum et al., 1998a, 1998b, 1999) and solution NMR data (Mizoguchi et al., 1996, 1998) of chlorosomes and Bchl *c* aggregates, respectively. In this arrangement, the smallest unit of the self-aggregated structures consists of the Bchl molecules organized into stacks. Several of these stacks (the number of stacks per rod depends on the species) form rod-like suprastructures by forming a hydrogen-bonding network. Several of these rod-like structures, organized hexagonally in 2 or 3 layers, make up the interior of a chlorosome (Staehelin et al., 1978, 1980). We use this hierarchical aggregation principle here to build up the structural units for our exciton calculations. The main differences in the structural organization of chlorosomes from the bacteria *Cf. aurantiacus* and *Cb. tepidum* are the diameter of the rod-like aggregates (~5.2 nm vs. ~10 nm) and the period of two-dimensional hexagonal lattice (ca. 6 nm vs. 10 nm).

In the present work, we have explored the exciton dynamics and energy transfer pathways at low temperature in two types of chlorosomes mostly by means of photon echo (PE) spectroscopy, supplemented partly by TA spectroscopy. The measurements were performed by using the so-called two-pulse PE technique (for details see Mukamel, 1995, p. 289). In simple terms, this method measures the decay of the coherence of the excited state, created by a coherent light pulse. Unlike TA spectroscopy, this technique is more informative and more sensitive to the detailed structural organization of identical pigments in a supramolecular aggregate structure. This important advantage thus gives the possibility for revealing the role of the superlattice-like organization of the Bchl aggregates in the exciton relaxation and energy transfer processes. For direct measurements of the population relaxation kinetics, the one-color TA-spectroscopy has been used. The experimental data are interpreted within a theoretical model based on the recently proposed model of the self-organized Bchl *c* aggregate rods (Holzwarth and Schaffner, 1994).

MATERIALS AND METHODS

Sample preparation

Cb. tepidum ATCC 49652 and *Cf. aurantiacus* OK70fl, DMS636 were grown in the media described in Wahlund et al. (1991) and Griebenow and Holzwarth (1989), respectively. Both strains were cultivated in continuous cultures in 1-liter bottles in order to obtain a homogeneous sample. The cultures were illuminated continuously with three 60-W light bulbs for *Cb. tepidum* and three 40-W bulbs for *Cf. aurantiacus* at a distance of 10 cm from the surface of the culture vessel. For *Cb. tepidum* the dilution rate was 0.25 day^{-1}, resulting in OD of 6.7 cm^{-1} in the Q_y absorption maximum and 90 nmol BChl *c* per milliliter of cell culture. The corresponding values for *Cf. aurantiacus* were 0.3 day^{-1}, 1.2 cm^{-1}, and 8 nmol ml^{-1}. Cells were harvested by centrifugation for 20 min at 2300 × *g* and stored at −20°C. Chlorosomes were prepared as described (Steensgaard et al., 1997) except that TX-100 was omitted and 20 mM potassium-phosphate buffer, pH 7.4, was used instead of Tris-HCl. Chlorosomes were stored at −40°C until further use. For measurements the chlorosomes were diluted in 20 mM potassium-phosphate, pH 7.4, containing 60% glycerol to OD ~ 12 cm^{-1} in the aggregate Q_y band. About 20 mM sodium dithionite was added and the sample was incubated for 2 hours at room temperature in the dark under anaerobic conditions. The 0.5-mm-thick cell of 15 μm volume was filled in the dark under a nitrogen atmosphere and slowly cooled to 4.2 K by immersing it in an optical bath cryostat model B29 (Institute of Physics, Kiev, Ukraine) filled with liquid helium. The cryostat pumping system allowed measurements in the range of 1.25 to 4 K for a period of 15 to 18 hours. The temperature was controlled by the vapor pressure of the helium atmosphere and was measured by a calibrated semiconductor transducer with an accuracy of ±0.01 K. Absorption spectra were recorded at room temperatures on Unicam UV2 (Spectronic Unicam, Cambridge, UK) and at 4.2 K (directly in cryostat) on Omega-10 (Bruins Instruments, Puchheim, Germany) spectrophotometers. The absolute maximum of absorbency in the Q_y absorption region was about 1.

Time-resolved spectroscopy

All time-resolved measurements were carried out at 1.27 K with the same optical setup shown schematically in Fig. 1. The commercial Ti:Sapphire

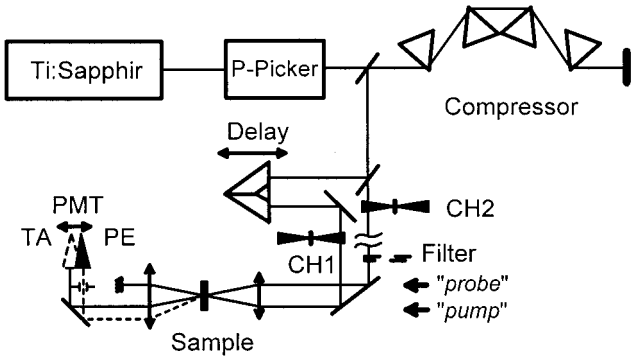

FIGURE 1 Schematic representation of the experimental setup for the 2PE and TA measurements. Ti:Sapphir, laser; P-Picker, pulse picker; CH1 and CH2, mechanical choppers; PMT, photomultiplier; TA and PE, locations of the PMT by transient absorption and photon echo measurements, respectively.

self-mode-locked femtosecond laser model Tsunami (Spectra Physics, Mountain View, CA) allowed to produce transform-limited ≈60-fs pulses with spectral FWHM ~12 nm at 790 nm, measured before the pulse picker, in the range 725–860 nm with a 80 MHz repetition rate. For decreasing the repetition rate to 80 kHz, a pulse picker model 3980 (Spectra Physics) was installed. Double passing of the laser beam through four SF10 prisms performed compensation of chirp that arises in the pulse picker and in the other optical elements. The FWHM of cross-correlation function (CCF), measured by non-collinear second harmonic generation in the KDP crystal, was 140 fs, corresponding to Gaussian-shaped pulses of 90 fs. The CCF was measured concurrently with every PE and TA scan. The two-pulse PE and one-color TA studies were carried out in the typical pump-probe setup. In the PE measurements the energy ratio of pump-probe pulses was 1:1.2 and for TA measurements it was 50:1. The photon echo signal was registered in the $k = 2k_1 - k_2$ direction by a photomultiplier (PMT) R374 (Hamamatsu, Hamamatsu City, Japan). In order to obtain the PE data in absolute units the PMT spectral sensitivity was calibrated. Switching between PE and TA measurements was realized on the same sample by moving the PMT and placing the neutral density filter (T = 2%, Balzers, Bal-tec, Lichtenstein) into the probe-beam. The probe pulse was delayed by a delay line with a minimal step size of 1 μm. The beams were focused into the sample by a lens with focal length of 150 mm to a diameter of approximately 150 μm. The angle between the crossed pump and probe beams with equal polarization was 25 mrad. After the sample, the beams (pump, probe, and the PE) were collimated by a lens with focal length of 100 mm and directed to the PMT after filtering through an aperture. The maximum available pump energy was 300 pJ/pulse, corresponding to a density of excitation energy $\leq 6 \cdot 10^{12}$ phot/cm^2 per pulse. At these conditions annihilation was not observed as shown in Fig. 2; note that the OD is normalized for both curves. (Annihilation may occur in the pigments belonging to the base plate at those intensities. Such an annihilation, if it does indeed occur, though this has not been checked by us, would be irrelevant in the context of this paper.) For noise suppression, a double lock-in technique was applied and a spatial filter was used before the PMT. Two mechanical choppers with frequencies of 273 and 146 Hz modulated the pump and probe beams. For an averaging time of 1 s per point, the absolute sensitivity of the PE setup was approximately 5 photons/pulse. The decay traces were measured in several delay scan ranges: 6 ps with a delay step of 27 fs for the PE and TA in both chlorosomes, 50 and 100 ps with delay step of 106 and 217 fs for the PE in *Cf. aurantiacus* and *Cl. tepidum*, respectively. The TA kinetics were measured also in the scan range of 100 ps (delay step 217 fs) for both types of chlorosomes.

Analysis of the decay traces was carried out independently for each wavelength by using a deconvolution procedure in a multiexponential

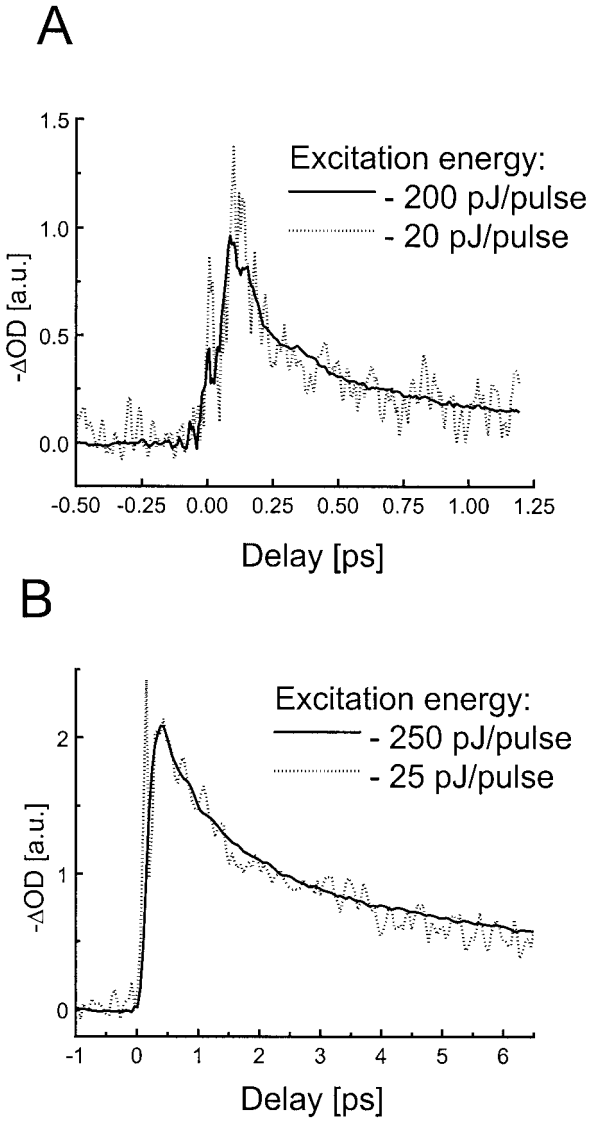

FIGURE 2 Check of annihilation-free conditions: decay of induced bleaching in chlorosomes of *Cl. tepidum* at 760 nm (*A*) and 770 nm (*B*) at different excitation energies.

fashion:

$$S(\tau) = \sum_i S(\tau_i)P(t - \tau) \otimes \exp(-t/\tau_i) \qquad (1)$$

where $S(\tau)$ denotes a measured signal (PE or TA), τ is the delay time between the pump and probe pulses, $P(t - \tau)$ is the pulse envelope, symbol $\otimes$ denotes a convolution integral, τ_i corresponds to the *i*th decay constant, and $S(\tau_i)$ is the amplitude. If τ_i is longer than the pulse duration or comparable to it, this expression can be simplified to:

$$S(\tau) \cong \sum_i S_i \exp(-\tau/\tau_i) \int_{-\infty}^{\tau} [CCF(t)]^{1/n} dt \qquad (2)$$

where n ≡ 1, 2 for TA and PE measurements, respectively. For the TA decays recovered in such a manner the decay constants τ_i correspond to the population relaxation times $(T_1)_i$, and in the PE case they are related to the dephasing times $(T_2)_i$ as $\tau_i = (T_2)_i/4$ (Allen and Eberly, 1975). The number of relevant decay components was estimated from the lifetime spectra, obtained by numerical inverse Laplace transform (NILT) of the measured decay traces (see Appendix A). This technique was applied only for analysis of decay traces measured over the wide decay windows. The recovered amplitudes of the PE signals were absorption corrected by using Eq. B8 (see Appendix B). The averaged decay constants were calculated using the standard expression:

$$(\tau_i)_{av} = \sum_k S_i(\lambda_k)\tau_i(\lambda_k) \Big/ \sum_k S_i(\lambda_k), \qquad (3)$$

where $S_i(\lambda_k)$ is the amplitude of the ith decay constant at the kth wavelength.

RESULTS

Photon echo measurements

The PE signal has been observed over a relatively wide spectral range (740–780 nm) for *Cl. tepidum* chlorosomes but in a much narrower region (only 735–755 nm) for the *Cf. aurantiacus* chlorosomes. Despite identical experimental conditions, the PE intensity from *Cf. aurantiacus* chlorosomes was about 1.5 times higher. This allows us to conclude that the dipole strength of the excited excitonic transitions in *Cl. tepidum* chlorosomes is higher than in *Cf. aurantiacus* chlorosomes. Analysis of the PE traces (dephasing decays) performed by the NILT technique shows that the dephasing times are not strongly distributed. For the chlorosomes from both bacteria, these narrow dis-

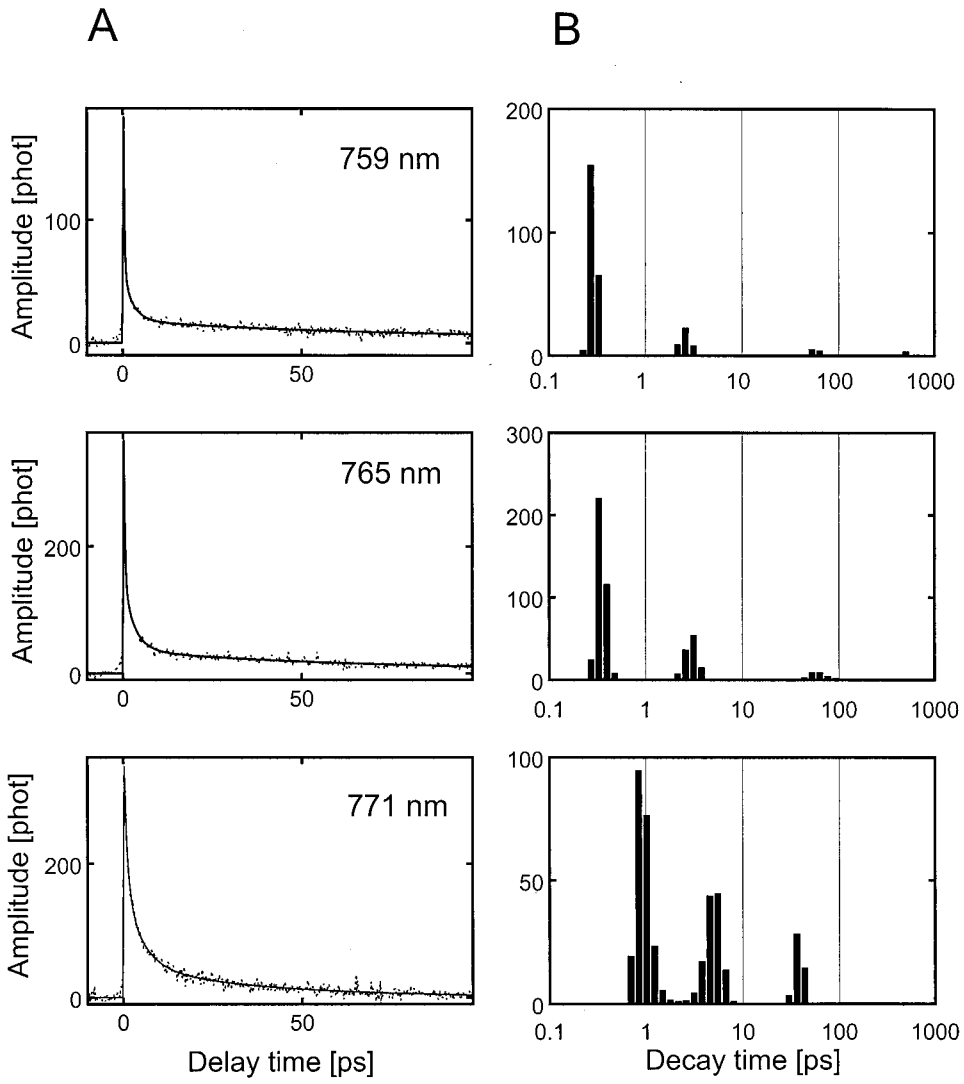

FIGURE 3 Dephasing traces (*A*, solid—fit, dotted—measured) and corresponded dephasing decay-time spectra (*B*) in chlorosomes of *Cl. tepidum* at different wavelengths.

tributions imply mainly a discrete character of the decays. In Fig. 3 the decay-time spectra for *Cl. tepidum* at several measuring wavelengths are shown as an example (note that the dephasing times are four times longer; see above). The decay components faster than 100 fs cannot be resolved in this delay window due to the relatively coarse delay step. From the discrete character of the dephasing time distribution, one can conclude that the spectrum of the exciton states in the first exciton band should also have a discrete nature. Figure 4 shows the wavelength distribution of the dephasing times for the *Cl. tepidum* chlorosomes, plotted on a semilog scale. The wavelength dependency of the dephasing times displays oscillation-like behavior. The averaged dephasing times for chlorosomes from both bacteria are collected in Table 1. One recognizes basically four groups of dephasing times T_2, stretching from ~100 fs up to 300 ps, which are similar for both types of chlorosomes. These components reflect the different exciton dephasing, exciton relaxation, and energy transfer processes. We assign the slowest dephasing to the energy transfer from the chlorosomal aggregates to the base plate. Assuming inhomogeneous broadening the chlorosome → base plate energy transfer times are ≈140 ps and ≈45 ps for the *Cl. tepidum* and *Cf. aurantiacus*, respectively. The absorption-corrected amplitude distributions for the different dephasing components are plotted in Fig. 5. These distributions differ strongly for the two chlorosome types. Firstly, the dephasing spectrum of the *Cf. aurantiacus* chlorosomes is very narrow and its FWHM is comparable to the FWHM of the laser light spectrum. Secondly, for the *Cl. tepidum* chlorosome the 1-ps dephasing component has an asymmetrical shape and clearly displays an oscillation structure (three maxima can be resolved at 745, 755, and 770 nm). The other components show a more bell-like shape. The 140-fs component in the *Cl. tepidum* dephasing spectrum can be fitted to a Gaussian profile with FWHM of 430 cm^{-1}, whereas a Gaussian fitting of the 8.3-ps component in the *Cf. aurantiacus* dephasing spectrum results in a FWHM of ~210 cm^{-1}.

TABLE 1 Average dephasing times T_2 for chlorosomes from the green bacteria *Cl. tepidum* and *Cf. aurantiacus*

Dephasing component	*Cl. tepidum*	*Cf. aurantiacus*
very fast	140 fs	280 fs
fast	1 ps	1.4 ps
middle	10 ps	8.3 ps
slow	280 ps	96 ps

Transient absorption measurements

In order to better understanding of the exciton dynamics in the chlorosomes, the corresponding one-color TA measurements were performed with the same samples and at the same experimental conditions as the 2PE measurements. The population dynamics were measured for the *Cl. tepi-*

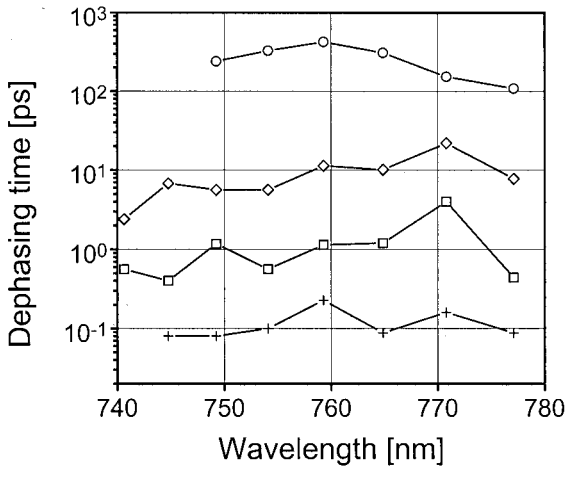

FIGURE 4 Wavelength distribution of dephasing times T_2 in *Cl. tepidum* chlorosomes (+, very fast; □, fast; ◇, middle; ○, slow component, respectively).

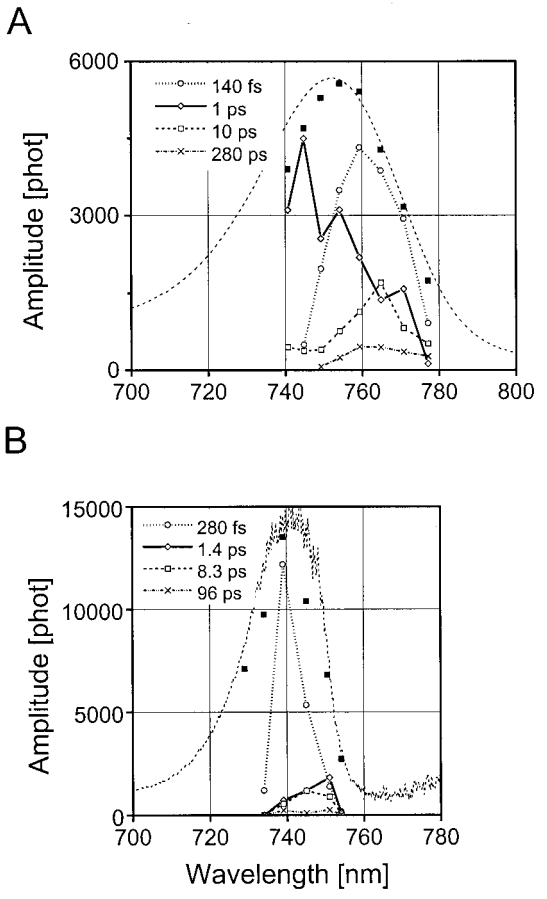

FIGURE 5 Amplitude distributions of recovered dephasing times for *Cl. tepidum* (*A*) and *Cf. aurantiacus* chlorosomes (*B*). For comparison the absorption spectra are also shown (dotted—measured with spectrophotometer: *Cl. tepidum* at 300 K, and *Cf. aurantiacus* at 4.2 K; boxes—with laser in situ at 1.27 K).

dum at 759, 771, and 781 nm and for *Cf. aurantiacus* chlorosomes over the whole Q_y band. At identical experimental conditions the maximal bleaching in the TA traces for *Cf. aurantiacus* was about 5 times higher than for *Cl. tepidum* chlorosomes. This means that the square of dipole strength (μ^2) is accordingly higher. This assumption is in agreement with the PE data. At wavelengths shorter than 740 nm in the chlorosomes from both bacteria a strong excited-state absorption was detected, in agreement with previous observations (Psencik et al., 1998; Savikhin et al., 1998). Figure 6 presents the absorption difference spectrum for *Cf. aurantiacus* chlorosomes, detected at a time delay of 150 fs. Comparing this to the dephasing spectrum (Fig. 5 *b*) reveals that a PE signal is generated only in the excited-state absorption free region of the Q_y band. This situation was qualitatively analyzed in van Burgel et al. (1995), where it was demonstrated that the contribution of higher exciton zones to the PE signal has destructive character. Accordingly, we suggest that the strong excited-state absorption completely suppresses the PE in our case.

Analysis of the measured TA decays by means of the numerical inverse Laplace transform method (decay-time spectra are not presented) shows the analogous features in the decay-time spectra; the population relaxation lifetimes are also discrete rather than being distributed. In Table 2 the T_2 and T_1 times for both types of chlorosomes are compared at wavelengths that correspond to the maximal bleaching in the TA. It can be seen that in both types of chlorosomes the relation T_2/T_1 is equal to 2/1 (the deviations for the slow decay component can be explained by a relatively high contribution of pure dephasing). This ratio depends on the nature of the broadening: for inhomogeneous broadening $1/T_2 = 1/2T_1 + 1/T^*$ and, for a homogeneously broadened system, $1/T_2 = 1/T_1 + 1/T^*$ (Joo and Albrecht, 1993). The pure dephasing time T* at low temperatures was not directly measured for chlorosomes, but for J aggregates it is usually much longer than T_2, and at 1.27 K it can be estimated to be nanoseconds (de Boer et al., 1987). Thus, we can assume

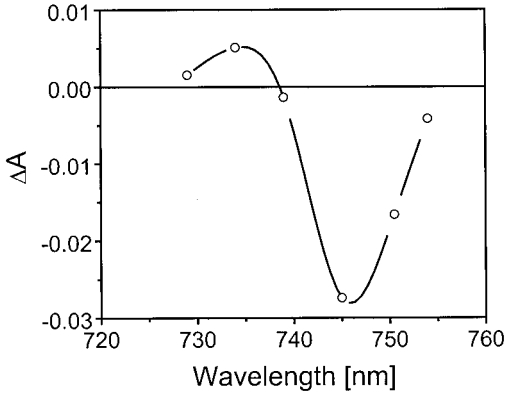

FIGURE 6 Absorption difference spectrum in the *Cf. aurantiacus* chlorosomes at time delay of 150 fs.

TABLE 2 Comparison of recovered dephasing times T_2 and relaxation population times T_1 for the investigated chlorosomes

Cl. tepidum @ 759 nm		*Cf. aurantiacus* @ 745 nm	
T_2	T_1	T_2	T_1
600 fs	280 fs	212 fs	160 fs
2.2 ps	1 ps	2.3 ps	1 ps
12.4 ps	5.8 ps	12 ps	5.4 ps
240 ps	115 ps	180 ps	127 ps

that the photon echo at low temperatures is purely determined by the population relaxation processes and the aggregates in chlorosomes from both bacteria seem to be inhomogeneously broadened, in good agreement with the previous HB data (Fetisova and Mauring, 1992, 1993; Psencik et al., 1994, 1998).

The delocalization of excitation in chlorosomes (in other words, the number of excitonically coupled pigments) can be also estimated from the TA data. Because of delocalization of the excitation over many pigments, the square of the dipole strength for delocalized transition should be much higher and roughly proportional to the sum of the square of the dipole strengths allowed in transition pigments. For one-color pump-probe spectroscopy in the absence of excited-state absorption and in the low-excitation limit the maximal bleaching ΔA around zero delay (for $\tau < T_2$) is proportional to the excitation energy E_{pump} and to the absorption cross-section σ of excited transition as (Prokhorenko et al., 1983):

$$\frac{\Delta A}{A} = -2\sigma E_{pump} \tag{4}$$

where A is absorbence and the coefficient 2 is due to contribution of stimulated emission. (The absorption cross-section is related to the extinction coefficient $[\epsilon]$ = liter/M · cm as $\sigma = 3.824 \cdot 10^{-24}\epsilon$ and $[\sigma] = cm^2$.) From this expression it follows that the average number of coupled pigments can be estimated as:

$$N_{delocal} \approx \frac{\sigma}{\sigma_0} \equiv -\frac{1}{2\sigma_0 E_{pump}} \frac{\Delta A}{A}, \tag{5}$$

where σ_0 is the absorption cross-section of a single pigment. For Bchl *c*, $\sigma_0 \approx 2.9 \cdot 10^{-16}$ cm^2 in the maximum of the Q_y absorption band (Stanier and Smith, 1960; Oelze, 1985). The experimental conditions are listed in Table 3. The maximal bleaching corresponds to a delay time of ≈100 fs. Based on these data the estimations show that the excitation is delocalized over 2 to 3 pigments in *Cl. tepidum* chlorosomes and over 10 to 12 pigments in the *Cf. aurantiacus* chlorosomes. This degree of delocalization in the *Cf. aurantiacus* chlorosomes is in reasonable agreement with previously published values, derived from TA measurements at room temperatures (Savikhin et al., 1998). For *phaeobacte-*

TABLE 3 Parameters (*top*) used in the estimation of the excitonically coupled pigment number $N_{delocal}$ (*bottom*) in chlorosomes

Parameter	*Cl. tepidum*	*Cf. aurantiacus*
λ_{max} (nm)	760	745
$A(\lambda_{max})$	0.78	0.8
$\Delta A(\lambda_{max})$	−0.005	−0.027
E_{pump} [phot/cm^2]	$4 \cdot 10^{12}$	$5.5 \cdot 10^{12}$
σ [cm^2]	$8 \cdot 10^{-16}$	$3.1 \cdot 10^{-15}$
$N_{delocal}$	2 ÷ 3	10 ÷ 12

roides chlorosomes, which are structurally similar to the *Cl. tepidum* ones, the number of coupled pigments was estimated from time-resolved fluorescence measurements to be 2 to 3 at 77 K (van Walree and Holzwarth, personal communication), which is also in agreement with our estimations.

Oscillations in the kinetics

Oscillations were observed in the TA and PE signals in both types of chlorosomes. They have similar features to that observed earlier. The oscillatory-like modulations of the signals depend on the wavelength and their relative contribution is maximal at the maximum of the PE spectrum. Figure 7 presents the decay traces of the TA and PE signals recorded around zero delay. It can be seen that the oscillations in the PE and TA signals have roughly equal periods and amplitudes for *Cl. tepidum*, but for *Cf. aurantiacus* chlorosomes, they are much stronger in the PE signal. A Fourier analysis of the residuals (difference signal to the exponent decays) resulted in main frequencies of ~70 cm^{-1} and ~160 cm^{-1} for *Cl. tepidum* and ~50 cm^{-1} and ~200 cm^{-1} for *Cf. aurantiacus* chlorosomes. These numbers are in agreement to the frequencies, which were observed previously (see Introduction) at room temperatures. The presence of these oscillations in the TA and PE signals simultaneously allows us to conclude that the origin of these oscillations is intramolecular vibronic states (or coherent nuclear motions, see Mukamel, 1995, p. 305 and p. 219) rather than quantum beats between closely spaced exciton levels, because the quantum beats would not change the degree of coherence in the coherently excited system.

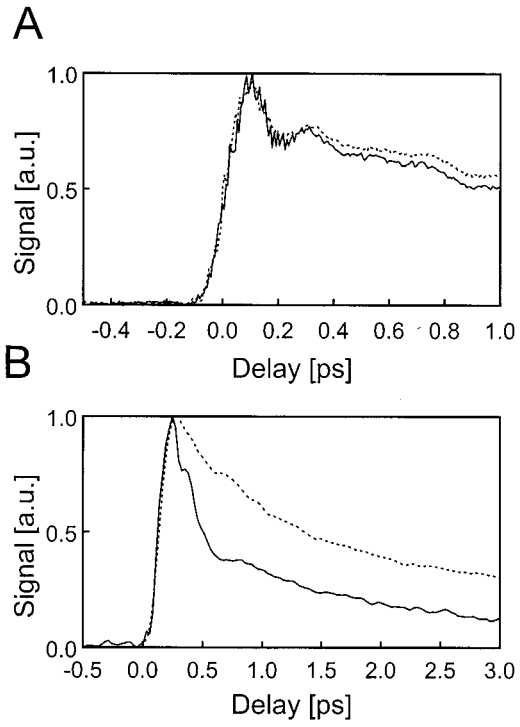

FIGURE 7 Oscillations in the PE (*solid line*) and TA (*dashed line*, −ΔA) signals from the *Cl. tepidum* (*A*, 771 nm) and *Cf. aurantiacus* chlorosomes (*B*, 751 nm). Signals are normalized to 1 in maxima.

MODELING OF THE OPTICAL PROPERTIES

In this section, we will confine ourselves to modeling of the steady-state spectroscopic properties of the single rod-aggregates and of arrangements of closely packed rods, as present in the chlorosomes. A detailed kinetic modeling of the exciton relaxation and energy transfer processes would require knowledge about the so-called system-bath correlation function of the pigments in the aggregates and their electron-photon coupling strength. Unlike protein-containing antenna complexes, these important parameters are still unknown for the protein-free self-organized aggregates of Bchls. However, some important features that result from the modeling of the steady-state spectra can also explain to a large extent our time-resolved experiments.

Structural model

For the modeling of the optical properties of chlorosomes the structural information on the aggregate, as derived previously (Holzwarth and Schaffner, 1994), was used. The published model was actually derived for the Bchl *d*. Recent calculations by molecular modeling showed that the same structures and orientations are valid for the Bchl *c* (Steensgaard and Holzwarth, unpublished). Thus, only the curvatures of the rods have been adapted to achieve the rod diameters as obtained from the electron microscopy (Staehelin et al., 1978, 1980). The main organization principle is self-organization of the Bchl *c* molecules to a supramolecular aggregate. Briefly, this calculated model system contains 90 Bchl molecules, arranged into 18 stacks, each rotated by 20° and finally forming a tubular micelle, i.e., a rod aggregate (Figure 8). (A stack is defined by a group of Bchls connected via the OH—Mg– bonds as shown in Fig. 8. The *Z*-axis corresponds to the stack axis and is also parallel to the rod axis. In calculated structure each stack contains 5

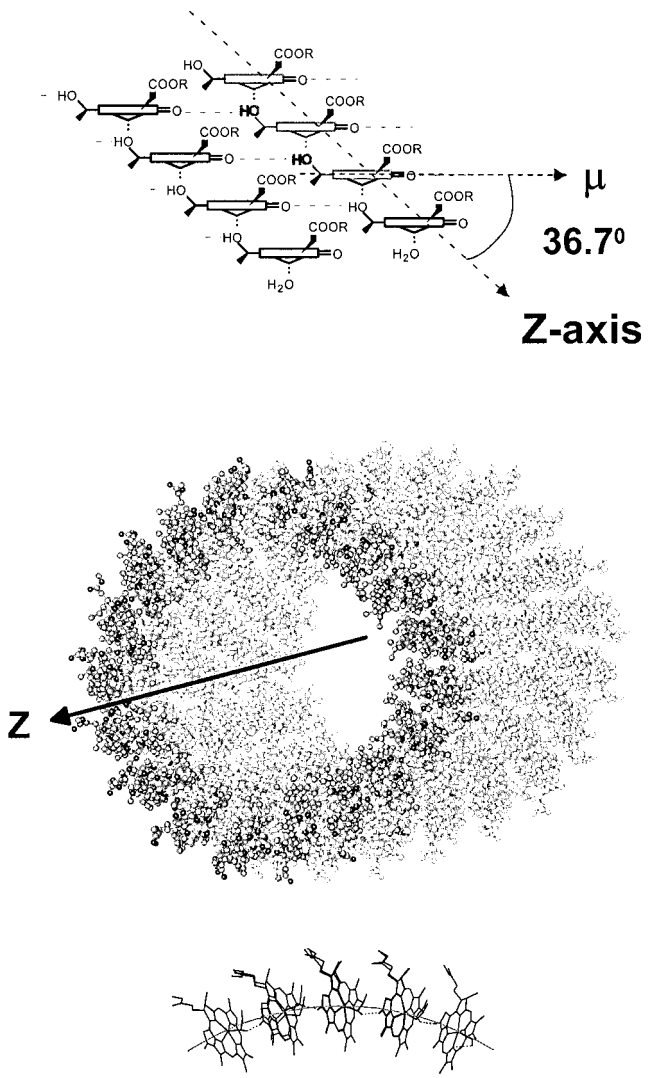

FIGURE 8 Space view of the tubular Bchl *c* aggregate, obtained by molecular modeling calculations (extended from Holzwarth and Schaffner, 1994). The farnesyl groups, pointing to the outside of the rod, are not displayed. The arrangement of Bchls in a stack is shown on the top. The dashed *Z*-axis connects the Mg-atoms of the Bchls in a single stack. Note that this axis also parallel to the rod axis.

Bchls.) Each stack is shifted along the rod axis by 2.16 Å with respect to its neighbors. This shift corresponds exactly to ⅓ of the distance between neighbors in a stack. Thus, the pigments form a two-dimensional lattice that is wrapped into a tube structure. The farnesyl groups in this aggregate are directed outside from the tube (like an inverted micelle). All derived structural parameters, which are important for modeling of the optical properties, are listed in Table 4. As can be seen, the geometry of this aggregate corresponds well with the aggregates from the *Cf. aurantiacus* chlorosomes (Staehelin et al., 1978). For modeling of the aggregate from *Cl. tepidum* chlorosome the number of stacks was increased up to 36, thus providing a rod diameter of 91.8 Å.

TABLE 4 Structural parameters of the Bchl *c* aggregates (based on Holzwarth and Schaffner, 1994), symmetrized to eliminate small deviations from the molecular modeling

Diameter (with respect to Mg-atoms)	45.94 Å
Distance between chlorins in stacks (Mg-Mg atoms)	6.5 Å
Shift between neighbors stacks	2.16 Å
Angle between μ* and symmetry axis (*Z*) of aggregate	36.7°
Angle between μ and radius-vector that crossed Mg-atom and *Z*-axis	80.4°

*The transition dipole moment of the BChl *c* molecule was defined as a vector connecting the C^{13} and Mg atoms.

The orientation of the transition dipole moments within the stacks and the other structural parameters (stack shift and distance between pigments in a stack) were not changed.

Spectra

The calculations of the absorption, circular dichroism (CD) and linear dichroism (LD) spectra of the excitonically coupled aggregates have been carried out using the Frenkel Hamiltonian without taking into account electron-phonon coupling. The dipole-dipole interaction energy $J_{i,k}$ between the *i*th and *k*th pigment was calculated in the point-dipole approximation:

$$J_{i,k} = \frac{\vec{\mu}_i \cdot \vec{\mu}_k}{|\vec{R}_{ik}|^3} - 3\frac{(\vec{\mu}_i \cdot \vec{R}_{ik})(\vec{\mu}_k \cdot \vec{R}_{ik})}{|\vec{R}_{ik}|^5}. \quad (6)$$

Here $\vec{\mu}_i$ corresponds to the transition dipole moment of *i*th pigment and $\vec{R}_{ik}$ is the distance vector between the *i*th and *k*th pigment, defined with reference to the Mg atoms (Agranovich and Galanin, 1982). For the dipole strength we use the value for the free Bchl *c*, because the regular tightly packed pigments in aggregates are close to a molecular crystal structure rather than to an impurity centers approach. For the latter, a correction for the specific dielectric constant of the host matrix would be required (Agranovich and Galanin, 1982). The value of the squared dipole strength ~ 30 D^2 was estimated from the published data for the extinction coefficient (Stanier and Smith, 1960; Oelze, 1985) and from the shape of the Q_y absorption band of Bchl *c* in acetone using the well-known relation (Houssier and Sauer, 1970). The calculated interaction energies are quite high: for the neighbors within a stack it is -511 cm^{-1} and for the neighbors between parallel stacks it is ≈ 200 cm^{-1}. For calculating the absorption, CD, and LD stick-spectra, the expressions from Pearlstein (1991) were used, assuming the 0–0 transition at $\lambda_{00} = 670$ nm, close to the maximum of the Q_y monomer absorption band. For calculating the LD spectrum, the direction of the macroscopic symmetry axis (and thus the orientation) was assumed to be parallel to the symmetry axis of the aggregate rods.

Stacks and rods

Figure 9 presents the absorption spectra of single stacks for different stack lengths (N_{stack} is number of Bchls in a single stack). It can be seen that the aggregation red shift is strong and saturates at ~10 pigments in a stack at ≈1900 cm^{-1}. In Fig. 10 the spectra for single rods for the *Cf. aurantiacus* and *Cl. tepidum* chlorosomes, calculated for $N_{stack} = 8$, are shown. Interaction between the stacks in an aggregate leads to the partial removal of the degeneracy of the lowest exciton state because of splitting and further increases the red shift. The aggregation shift in aggregates saturates of ~8 pigments in a stack. The splitting is quite different despite the similar interaction energies between pigments in both types of chlorosomal rod aggregates. The lowest exciton state is split by 88 cm^{-1} and by 53 cm^{-1}, respectively, for the *Cf. aurantiacus* and *Cl. tepidum* aggregates. However, these split states are still degenerate. The maximum of absorption spectrum for both aggregates is located around 750 nm, which is in agreement with experimental observations. Thus, we can conclude that the dipole-dipole interaction in the ground state is negligibly small as compared to the interaction in the excited state. The shapes of the calculated CD and LD spectra correspond very well to the measured ones (see, e.g., Griebenow et al., 1991; Olson et al., 1990). (Largely different CD spectra have been published for chlorosomes from various organisms (Olson et al., 1985; Brune et al., 1990; Griebenow et al., 1991; Wang et al., 1995; Steensgaard et al., 2000; Frese et al., 1997; Lehmann et al., 1994; Ma et al., 1996b). It had been proposed that these varying CD spectra of chlorosomes from the same organism are actually due to a superposition of two types of spectra (Griebenow et al., 1991) and possibly also due to a substantial contribution from a PSI (polymer and salt induced)-type CD signal (Keller et al., 1986, Balaban et al., 1995). Ma et al. (1996b) could show for *Chloroflexus aurantiacus* that the type of CD observed depends on the light conditions during growth of the cells, actually changing roughly between the two extremes that had been proposed as type I and type II by Griebenow et al. (1991). This finding is consistent with the notion that the overall size of a chlorosome and also the relative composition of pigment components within the chlorosome is changing with the light conditions (reviewed by Blankenship et al., 1995) which in turn largely influences the CD. The CD that is calculated in this work corresponds closely to the CD of the high light grown cells (Ma et al., 1996b) and to the type I CD of membrane preparations of *Chloroflexus aurantiacus* (Griebenow et al., 1991). These chlorosomes are likely to be smaller in length and width than those of very low light cells, and thus contributions from PSI-type CD effects might be small or even absent (Balaban et al., 1995). Such PSI-type CD effects add to the intrinsic CD and can distort the observable CD strongly as compared to the intrinsic one if the dimensions of the particles are in the vicinity of the wavelength of light.) It should be pointed out that the presence of three clearly resolved sub-bands observed in the CD spectra can be explained well only in the framework of the present structural model, in which the stacks in an aggregate are periodically shifted relative to each other.

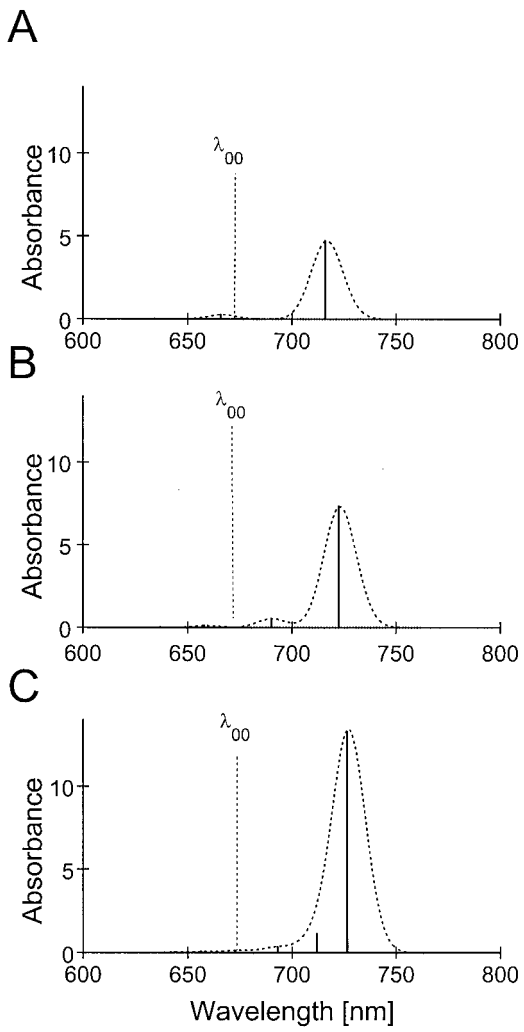

FIGURE 9 Calculated absorption spectra of single stacks for $N_{stack} = 5$ (*A*), 8 (*B*), and 15 (*C*), respectively. Stick-spectra are convoluted with Gaussian band FWHM = 350 cm^{-1}. Absorption is normalized to the value of μ^2 for a single Bchl *c*. Marker shows the position of the 0–0 transition.

Unit cell

In order to explore the role of the superlattice-like structural organization of the rods in chlorosomes we have analyzed the optical properties of a unit cell, which contains three hexagonally packed aggregate rods. From group theory it follows that for the analysis of the electronic structure it suffices to consider a single cell, because translation symmetry leads only to degeneration of the electronic levels. For calculations, the period of this unit cell was chosen in accordance with the electron microscopy data (Staehelin et

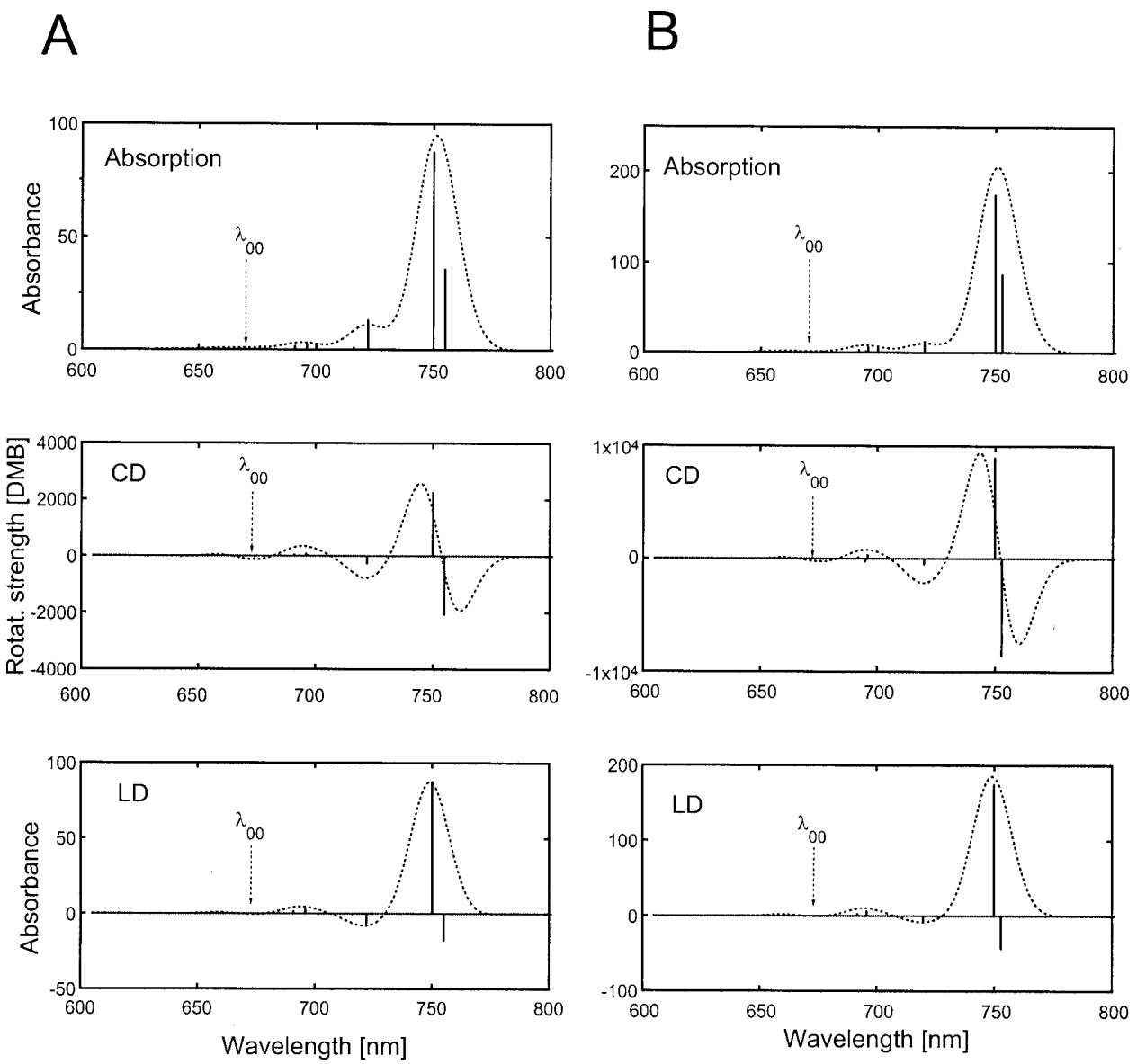

FIGURE 10 Calculated absorption, CD, and LD spectra of a single rod aggregate from the *Cf. aurantiacus* (*A*) and *Cl. tepidum* (*B*) chlorosomes. Stick-spectra are convoluted with a Gaussian band FWHM = 350 cm^{-1}. Absorbence scaling is the same as in Fig. 9.

al., 1978, 1980), to be 60 Å and 100 Å, respectively, for the *Cf. aurantiacus* and *Cl. tepidum* chlorosomes. Because of the very large number of Hamiltonian terms, these calculations were performed only for $N_{stack} = 7$, which should not influence the results substantially. The calculated absorption spectra for non-disordered unit cells are displayed in Fig. 11 *a*. The CD and LD spectra (not shown) demonstrate the same features as for the single aggregate rods. Hexagonal packing of rods in crystalline-like structure leads to a large splitting of the lowest exciton band, but the spectra differ strongly. For the *Cf. aurantiacus* chlorosomes, only two main sub-bands arise, whereas in the *Cl. tepidum* chlorosomes one obtains three equally spaced sub-bands. Increasing or decreasing of the unit cell period by increasing N_{stack} does not change these unique features. Analysis shows that the appearance of three sub-bands in the *Cl. tepidum* chlorosomes is due to a relatively weak curvature of the tubes as compared to the *Cf. aurantiacus* aggregates, which essentially leads to a greater number of coupled BChls between tubes.

Inclusion of disorder

Incorporation of the disorder (diagonal and off-diagonal) in the system does not change the main optical properties in comparison to a system with an ideal symmetry (as calcu-

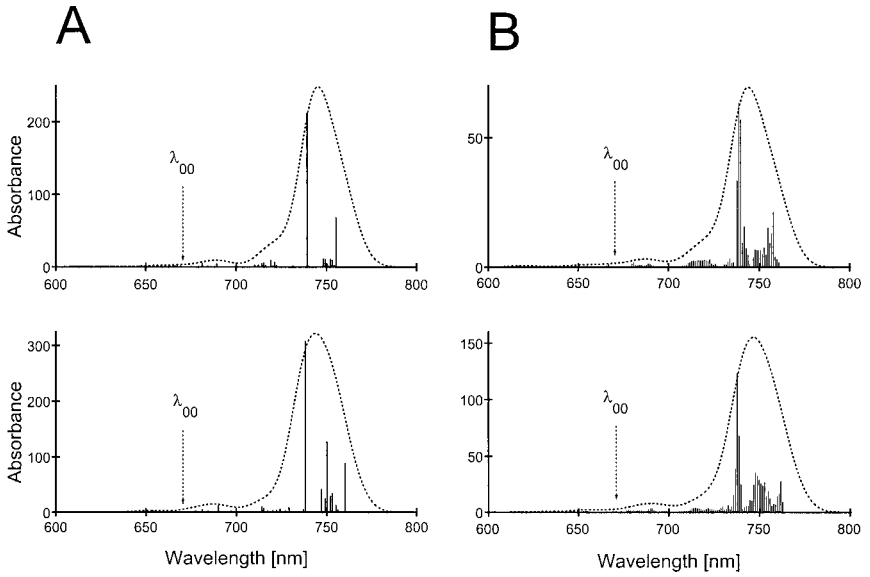

FIGURE 11 (*A*) Calculated absorption spectra of non-disordered unit cell of the *Cf. aurantiacus* (*top*) and *Cl. tepidum* (*bottom*) chlorosomes. (*B*) The same with off-diagonal disorder (for details see text). Stick-spectra are convoluted with Gaussian band FWHM = 350 cm^{-1}. Absorbence scaling is the same as in Fig. 9.

lated above). Figure 11 *b* presents calculated absorption spectra for the off-diagonal disordered ensemble of the unit cells (20 cells for *Cf. aurantiacus*, i.e., 60 rods, and 10 cells for *Cl. tepidum* chlorosome, i.e., 30 rods). The numbers of rods in the calculated systems correspond roughly to the native chlorosomes. The calculations were performed in the following way. For each single unit cell the appropriate interaction matrix was generated for the pigments, randomly distributed around their symmetrical positions and with randomly distributed directions of their dipole moments. The distribution was assumed to be normal with FWHMs as listed in Table 5. The deviations of the dipole moment directions and space positions of pigments were also estimated from the structure of modeled aggregate (Holzwarth and Schaffner, 1994). Then the spectra, independently calculated for each cell, were averaged over an ensemble. This modeling shows that the off-diagonal disorder leads to some decrease of the oscillator strength of the strongest transitions and to some spectral broadening, but qualitatively the spectra are not changed. The influence of diagonal disorder on the spectral properties was also analyzed. In accordance with PE experimental data, the FWHM for diagonal disorder was assumed to be ≈430 cm^{-1} and ≈210 cm^{-1} for the *Cl. tepidum* and *Cf. aurantiacus* chlorosomes, respectively. The calculated absorption spectra for diagonally disordered ensembles show similar spectral features as those for off-diagonally-disordered ensembles. Thus, disorder does not contribute substantially to the overall spectral properties within this approximation.

TABLE 5 Distribution for the pigment position and distribution of the dipole moment direction for calculations of non-diagonal disordered system

Disorder	Value of FWHM
along *X*-axis	0.3 Å
along *Y*-axis	0.3 Å
along *Z* (symmetry axis)	0.24 Å
of angle between $\vec{\mu}$ and *Z*-axis	10°
of angle between $\vec{\mu}$ and radius-vector	20.6°

DISCUSSION

As was mentioned above, the calculated absorption, CD, and LD spectra are in very good agreement with the measured spectra. These calculations are based on the structure of aggregates, obtained from molecular modeling (Holzwarth and Schaffner, 1994) and NMR spectroscopy (see Introduction). A different structural model of chlorosomal has previously been used for excitonic calculations (Novoderezhkin and Fetisova, 1996; Fetisova et al., 1996). In that model an aggregate consists of six linear stacks, assembled in a tubular structure with a low packing density. Besides not being based on any chemical or structural data, that model cannot explain the main features in the CD and LD spectra due to (i) the very low interaction energy between stacks and (ii) the absence of a periodical shift between stacks. The structural model on which this work is based, properly predicts the fine structure in the Q_y absorption region due to a splitting of the lowest exciton band (effect of super-lattice organization). Moreover, the presence of at least two sub-bands in the electronic structure of chlorosomes, which were tentatively assigned to different Bchl spectral forms, was pointed out earlier in several papers (Holzwarth et al., 1990b, and references therein; Griebenow et al., 1991; Psencik et al., 1994). It is now clear that the origin of this behavior is the interaction between hexagonally packed rod-like aggregates. This agrees with the time-resolved data. For instance, in the calculated absorption

spectrum of the *Cf. aurantiacus* unit cell (Fig. 11), the main sub-bands of the lowest exciton band are located at 739 nm and 755 nm and they are spaced by 16 nm. From comparison to the differential absorption spectrum (Fig. 6), it follows that the blue sub-band is completely overlapping the excited state absorption region. Therefore the PE signal is observed only from the red absorption sub-band and it should be spectrally narrow, which is in full agreement with the experimental observations. In the *Cl. tepidum* chlorosomes the calculated stick-spectrum of the unit cell displays a strong asymmetry and splitting into three sub-bands (~11 nm) which finds its experimental counterpart in the observed structure (spacing ~12 nm) in the spectrum of the 1-ps dephasing component (Fig. 5) which also shows a strong asymmetry. It should be pointed out that the structure in the wavelength dependence of the dephasing times (Fig. 4) is also correlated to these modulations in the calculated spectrum. Thus, we can conclude that the origin of the fine structure in the PE spectra is most likely due to an interaction between hexagonally packed aggregates. Moreover, the 1-ps dephasing component in the *Cl. tepidum* and the 680-fs component in the *Cf. aurantiacus* chlorosomes can be assigned to the fast energy transfer (more precisely to the energy redistribution) within a single rod aggregate. These dephasing times are similar to those obtained from HB spectroscopy studies (Fetisova and Mauring, 1992; Psencik et al., 1998). The middle dephasing component (which corresponds to $T_1 = 4–5$ ps; Table 1) should most likely be assigned to the energy transfer between different rod aggregates. Finally, the shortest dephasing time is caused by fast dephasing process in a single Bchl due to electron-phonon interaction, i.e., dissipation of excitation energy over the phonon bath. Therefore, its amplitude distribution shows a Gaussian shape (Fig. 5 *a*) with a relatively large FWHM. At room temperature this dephasing strongly accelerates and could be not resolved under our experimental conditions.

On the basis of both the experimental results and the model calculations, an energetic and kinetic scheme describing in detail the energy transfer pathways in chlorosomes can be proposed (Fig. 12). The energy transfer can be essentially divided into four steps. After excitation, an initially coherent excited state loses its coherence (at low temperatures with a dephasing time of ~150 fs) due to interaction with the phonon bath. In parallel, then, occur complex relaxation processes over a wide time range from ~100 fs to ~5 ps. Although we cannot strictly separate energy relaxation processes within a single rod from energy exchange among neighboring rods in the framework of an exciton model, some pieces of evidence nevertheless suggest that the slower part of this lifetime range (a few picoseconds) is essentially more related to energy exchange among rods than the faster part of that distribution. This is supported by time-resolved fluorescence data on special chlorosomes (Steengaard et al., 2000), where this process

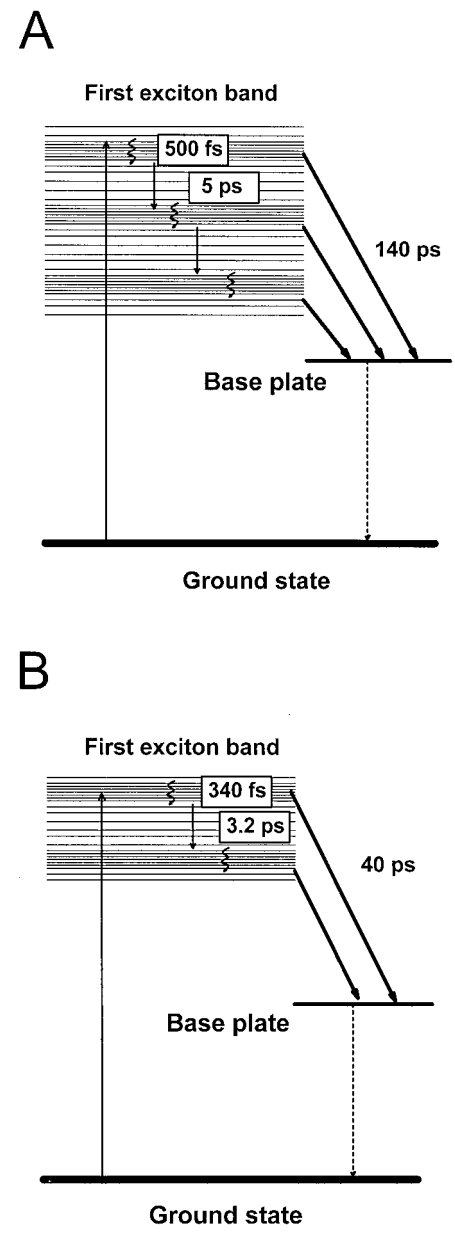

FIGURE 12 Proposed energetic and kinetic diagram for *Cl. tepidum* (*A*) and *Cf. aurantiacus* (*B*) chlorosomes. Here the averaged energy transfer times are shown. For details, see text.

can be resolved. Subsequently, energy located on the lower exciton states is, with a typical time of 140 ps (*Cl. tepidum*) and ~50 ps (*Cf. aurantiacus*) at very low temperatures, transferred to the base plate. At room temperature these transfer times speed up to about 40–60 ps (*Cl. tepidum*) and about 10–20 ps (*Cf. aurantiacus*; Savikhin et al., 1995a, 1996b; Causgrove et al., 1990; van Walree et al., 1999). This can be understood from the dipole strength distribution of the exciton states. The energy transfer to the base plate at room temperatures occurs from several exciton sub-bands.

CONCLUSIONS

Our structural model for aggregates and entire chlorosomes, based on the principle of self-organization (Holzwarth and Schaffner, 1994; Balaban et al., 1995; Nozawa et al., 1994; Mizogushi et al., 1998), describes very well the optical properties of native chlorosomes from both *Cf. aurantiacus* and *Cl. tepidum.* The model can be successfully used for a detailed kinetic modeling of the energy transfer processes in chlorosomes, which will be the subject of future work.

Modeling of the exciton structure as done in the present work shows that the interaction between closely packed rod aggregates, which form a two-dimensional superlattice-like structure in the chlorosomes, leads to a splitting of the lowest exciton band, which carries the largest dipole strength, and to the appearance of electronic fine structure in the Q_y absorption region. This fine structure is clearly manifested in the PE spectra.

The PE measurements and the resulting transfer lifetimes are in good agreement with values published previously, obtained by HB spectroscopy, TA techniques, and time-resolved fluorescence (Fetisova and Mauring, 1992; Psencik et al., 1998; Savikhin et al., 1994; Steensgaard et al., 2000; van Walree et al., 1999). In framework of the proposed energetic and kinetic diagram, all main experimental observations can be explained.

APPENDIX A

The measured decay traces can be described as a sum of a few exponential decays with different decay constants and different amplitudes (Eq. 2) or, alternatively, as a continuous distribution of exponential decays τ_{dec} with a continuous distribution of amplitudes $A(\tau_{dec})$:

$$S(\tau) = \left[\int_0^\infty A(\tau_{dec})\exp(-\tau/\tau_{dec})d\tau_{dec}\right]\int_{-\infty}^{\tau}[CCF(t)]^{1/n}dt. \quad (A1)$$

As can be seen from this expression, searching for the amplitude distribution $A(\tau_{dec})$, also called the decay-time spectrum, is related to inverse Laplace transform of the decay trace $S(\tau)$, deconvoluted with the response function CCF(t). This transform can be performed in a straightforward manner only if $S(\tau)$ is given as an analytical function. From the measurements $S(\tau)$ is usually given as a vector of real numbers, however:

$$s_k = S(\tau_k), \quad (A2)$$

where s_k is the signal magnitude at the kth delay point. This vector contains also a normally distributed noise component with mean 0. Therefore the transform can be performed by minimization of the function χ^2 (least-square fitting), defined as

$$\chi^2 = \sum_k (s_k - f_k)^2 \equiv \vec{r}^T\cdot\vec{r}, \quad (A3)$$

where f is a vector that corresponds to the model function, convoluted with the CCF(t). (For fluorescence decays the noise obeys a Poissonian distribution and this expression should be modified accordingly.) According to the exponential series method (James and Ware, 1986; Siemiarczuk et al., 1990; Landl et al., 1999) for the model function we have chosen a series of exponentials with fixed decay times T_i, equally spaced on a logarithmic scale:

$$T_i = T_{min}\left(\frac{T_{max}}{T_{min}}\right)^{\frac{i-1}{N-1}},$$
$$f_k = \left[\sum_{i=1}^{N} A_i\exp(-\tau_k/T_i)\right]\int_{-\infty}^{\tau_k}[CCF(t)]^{1/n}dt. \quad (A4)$$

The choice of the boundary conditions $[T_{min}, T_{max}]$ for the decay-time spectrum depends on the experimental situation. The minimal decay time T_{min} and the upper decay time T_{max} should be comparable to the delay step, and longer than the delay window by factor of 2 to 3, respectively. The number of components N in the decay-time spectrum is basically not limited by the number of experimental points and should be large enough to achieve the necessary resolution (usually ~50 exponentials). The last expression in Eq. A4 can be also given in vector form as $\vec{f} = \mathbf{M}\cdot\vec{A}$, and the residual vector is $\vec{r} = \vec{s} - \mathbf{M}\cdot\vec{A}$.

In PE experiments, one measures the degree of coherence in the excited state. This coherence can only decrease due to different dephasing processes (see Introduction); thus, we can assume that the decay-time spectrum must be positive and the elements of vector A can be given as $A_k = u_k^2$. In this case minimization of χ^2 can be performed by non-linear least-squares fitting (see, e.g., Fletcher, 1980). In this work for the calculation of $\chi^2(u)$ expansion into a Tailor series (quadratic approximation) is applied:

$$\chi^2(\vec{u} + \vec{\Delta}) \cong \chi^2(\vec{u}) + \vec{\Delta}^T[\vec{\nabla}\chi^2(\vec{u})] + \tfrac{1}{2}\vec{\Delta}^T[\vec{\nabla}^2\chi^2(\vec{u})]\vec{\Delta}, \quad (A5)$$

where the derivatives, determined by the chosen model function, are:

$$\vec{\nabla}\chi^2(\vec{u}) = \vec{g}(\vec{u}) = 2\mathbf{L}\cdot\vec{r};$$
$$\vec{\nabla}^2\chi^2(\vec{u}) = \mathbf{G}(\vec{u}) = 2\mathbf{L}\cdot\mathbf{L}^T + 2\vec{r}\vec{\nabla}^2\vec{r} \cong 2\mathbf{L}\cdot\mathbf{L}^T \quad (A6)$$

and $\mathbf{L}$ is the Jacobian matrix $\mathbf{L} = -2\mathrm{diag}(\vec{u})\cdot\mathbf{M}^T$. The search direction for $\vec{\Delta}$ is obtained by minimizing of χ^2 in Eq. A5 that leads to the solution of the linear system $\mathbf{G}(\vec{u})\cdot\vec{\Delta} = -\vec{g}(\vec{u})$, known as the Gauss-Newton method. A more stable solution is obtained using the Levenberg-Marquardt method in which the search direction can be precisely controlled by the parameter ν:

$$[\mathbf{G}(\vec{u}) + \nu\mathbf{I}]\cdot\vec{\Delta} = -\vec{g}(\vec{u}), \quad (A7)$$

where $\mathbf{I}$ is the identity matrix. This control is carried out by comparison of the predicted change $\delta\chi^2 = \chi^2(\vec{u}) - \chi^2(\vec{u} + \vec{\Delta})$ from Eq. A5 and that directly calculated from Eq. A3:

$$Pr(\nu) = \frac{\chi^2(\vec{u}) - \chi^2(\vec{u} + \vec{\Delta})}{-[\vec{\Delta}^T\cdot\vec{g}(\vec{u}) + \vec{\Delta}^T\cdot\mathbf{G}(\vec{u})\cdot\vec{\Delta}]}. \quad (A8)$$

For a stable iteration the value of Pr should be maintained around 0.7–0.8 (Fletcher, 1980). As a stop criterion for the iterative procedure, the criterion of achieving maximum entropy of χ can be used. This algorithm is working very stably and was intensively tested with numerous synthesized (with added noise) and measured decays and was compared to the trivial fitting proceeding with a few discrete exponentials (see Materials and Methods). This algorithm is also fully applicable for analyzing TA kinetics without rising components. For decay traces with positive and negative decay components the algorithm is still the same, only the model function f is changed; instead of the vector A the matrix $A_{k,m} = (-1)^m u_{k,m}^2$, where $m \in [0, 1]$, should be used, and the matrix M should be modified accordingly.

APPENDIX B

The PE light pulse is directly generated in a medium by sequentially applying two time-spaced laser pulses (so-called two-pulse PE) emanating into directions $\vec{k}_e = 2\vec{k}_2 - \vec{k}_1$ or $\vec{k}_e = 2\vec{k}_1 - \vec{k}_2$. Simultaneously with the PE generation, an absorption of the PE light pulse occurs in the same medium. Thus, for the samples with finite absorbency, a connection between the generated PE electrical field and the observed 2PE signal should be established. This relation can be found by analytically solving the Maxwell equation for the light propagation in the following approximations: (i) the pump/probe pulse energies are small, (ii) their spectral width $\Delta\omega_L$ is narrower as the full absorption spectral width, and (iii) the PE pulse energy is also very weak and does not affect the medium polarization. The wave equation for an electric field E in an isotropic medium can be written as:

$$\nabla \times \nabla \times \vec{E}(\vec{r}, t) + \frac{1}{c^2}\frac{\partial^2}{\partial t^2}\vec{E}(\vec{r}, t) = -\frac{4\pi}{c^2}\frac{\partial^2}{\partial t^2}\vec{P}(\vec{r}, t) \tag{B1}$$

where c is the light speed and $\vec{P}$ is a medium polarization. For the paraxial beams, the electric field in the medium can be given as the sum:

$$\vec{E}(\vec{r}, t) = (\vec{E}_1(z, t)e^{i\vec{k}_1\vec{r}} + \vec{E}_2(z, t)e^{i\vec{k}_2\vec{r}})e^{-i\omega_L t} + E_{echo}e^{i(\vec{k}_e\vec{r} - \omega_L t)} \tag{B2}$$

where indices 1,2 denote the pump and probe pulses, z is a longitudinal coordinate, and $E_{1,2}(z, t)$ are the pulse envelopes that are equivalent for the pump and probe pulses. The frequencies ω_L and ω_e correspond to the mean frequencies of the laser fields and the PE electric field, respectively. If the spectral width is narrower then the absorption spectrum of the sample, we can assume $\omega_L = \omega_e = \omega$. For the weak electric fields the polarization can be separated into linear and nonlinear parts $\vec{P}(\vec{r}, t) = \vec{P}_1(\vec{r}, t) + \vec{P}_{nl}(\vec{r}, t)$ and in our approximation (ii) $\vec{P}_1(\vec{r}, t)$ can be given in the form $\vec{P}_1(\vec{r}, t) = \chi^{(1)}(\omega)\vec{E}(\vec{r}, t)$ by using the linear response susceptibility $\chi^{(1)}$. The relation between $\chi^{(1)}$ and a dielectric function is $\epsilon = 1 + 4\pi\chi^{(1)}$, where $\sqrt{\epsilon} = n + ik$, $n \equiv n(\omega)$ is the refraction index and $k \equiv k(\omega)$ is an extinction coefficient. When the slowly varying amplitudes approach is applied, we obtain from Eq. B1 by selection of fields along their propagation directions according to their wave vectors:

$$\frac{\partial}{\partial z}E_{1,2}(z, t) = -\frac{\alpha}{2}E_{1,2}(z, t) \tag{B3}$$

which obeys the trivial solution for pump/probe pulses:

$$E_{1,2}(z, t) = E_{1,2}(0, t)\exp\left(-\frac{\alpha}{2}z\right). \tag{B4}$$

Here $\alpha \equiv \alpha(\omega)$ denotes the absorption coefficient, related to the extinction coefficient as $\alpha(\omega) \equiv k(\omega)N$ and N is the molar concentration of absorbers. Here we have neglected the interaction between pump and probe pulses in nonlinear media according to (i).

The nonlinear part of the polarization is the source of the PE. The standard procedure is expansion of $P_{nl}(r, t)$ in powers of the electric field. When the nonlinear response of the medium has a nonstationary character, then $P_{nl}(r, t)$ should be described as an integral function. In an isotropic medium the first term in the power series is a third-order field function (Shen, 1984) of the nonlinear response $\chi^{(3)}$:

$$\vec{P}_{nl}(\vec{r}, t) = \int_{-\infty}^{\infty} dt_1 \int_{-\infty}^{\infty} dt_2 \int_{-\infty}^{\infty} dt_3 \chi^{(3)}(t - t_1, t - t_2, t - t_3)$$
$$\vec{E}(t_1, \vec{r})\vec{E}(t_2, \vec{r})\vec{E}(t_3, \vec{r}) \tag{B5}$$

(here t_i denotes the independent time variables). Using again the slowly varying amplitudes approximation and (iii) we get from Eq. B1 an expression for the PE pulse propagation:

$$\frac{\partial}{\partial z}E_{echo}(z, t) = -\frac{\alpha}{2}E_{echo}(z, t) + i\frac{2\pi\omega}{nc}P_{nl}(z, t). \tag{B6}$$

The last term on the right hand side in Eq. B6 can be expressed by using Eq. B4 and B5 as $P_{nl}(z, t) = P_{nl}(t)\exp(-\frac{1}{2}\alpha z)$, and solution of Eq. B6 with initial condition $E_{echo}(0, t) = 0$ is:

$$E_{echo}(z, t) = i\frac{4\pi\omega}{nc}P_{nl}(t)\frac{\sinh(\frac{1}{2}\alpha z)}{\alpha}\exp(-\alpha z). \tag{B7}$$

This is a general expression for the electrical field of the PE pulse in the weak field limit for the medium with an arbitrary nature of the absorbance.

In the 2PE measurements we obtain a signal in the form of the time resolved spectra $SP(\omega, \tau) = (c/8\pi\hbar\omega)\int_{-\infty}^{\infty}|E_{echo}(d, \omega, \tau, t)|^2 dt$, here $SP(\omega, \tau)$ denotes the measured 2PE energy density and d is the path length in the cell. If the detector aperture is much larger than the echo irradiation divergence, the whole 2PE energy is measured and $SP(\omega, \tau)$ should be also integrated over the detector aperture. Eq. B7 allows one to pick out from the measured PE the particular dependency on the absorbency. In other words, it allows the normalization of the 2PE signal to the absorption spectrum of the sample. In experimental studies instead of α, the absorbency A is commonly used, which is related to the absorption coefficient as $A(\omega) = \alpha(\omega)d/\ln 10$. Then the normalization of the measured 2PE spectrum $SP(\omega, \tau)$ to the measured absorption spectrum $A(\omega)$ can be performed by the formula:

$$S_{2PE}(\omega, \tau) = \frac{2\hbar cn^2}{\pi\omega d^2}\left[\frac{2.303A(\omega)}{10^{0.5A(\omega)} - 10^{-0.5A(\omega)}}10^{A(\omega)}\right]^2 SP(\omega, \tau) \tag{B8}$$

This work was supported partly by Deutsche Forschungsgemeinschaft (Sonderforschungbereich no. 189), and by the European Community TMR project on green bacterial photosynthesis, grant no. FM RX-CT960081.

REFERENCES

Agranovich, V. M., and M. D. Galanin. 1982. Theory of electronic excitations in molecular crystals. *In* Electronic Excitation Energy Transfer in Condensed Matter, chapter 4. V. M. Agranovich, and M. D. Galanin, editors. North-Holland Publishing Company, Amsterdam. 81–170.

Allen, L., and J. H. Eberly. 1975. Optical Resonance and Two-Level Atoms, chapter 9. John Wiley and Sons, New York.

Balaban, T. S., A. R. Holzwarth, K. Schaffner, G. J. Boender, and H. J. M. de Groot. 1995. CP-MAS ^{13}C-NMR dipolar correlation spectroscopy of ^{13}C enriched chlorosomes and isolated bacteriochlorophyll *c* aggregates of *Chlorobium tepidum*: the self-organization of pigments is the main structural feature of chlorosomes. *Biochemistry.* 34:15259–15266.

Balaban, T. S., A. R. Holzwarth, and K. Schaffner. 1995. Circular dichroism study on the diastereoselective self-assembly of bacteriochlorophyll c_s. *J. Mol. Struct.* 349:183–186.

Balaban, T. S., H. Tamiaki, A. R. Holzwarth, and K. Schaffner. 1997. Self-assembly of methyl zinc (^{3}1R)- and (^{3}1S)-bacteriopheophorbides *d*. *J. Phys. Chem. B.* 101:3424–3431.

Blankenship, R. E., J. M. Olson, and M. Miller. 1995. Antenna complexes from green photosynthetic bacteria. *In* Anoxygenic Photosynthetic Bacteria. R. E. Blankenship, M. T. Madigan, and C. E. Bauer, editors. Kluwer Academic Publishers, Dordrecht. 399–435.

Brochon, J.-C. 1994. Maximum entropy method of data analysis in time-resolved spectroscopy. *In* Methods in Enzymology, vol. 240: Numerical computer methods. Bart, B., M. L. Johnson, and L. Brand, editors. Academic Press, San Diego. 262–311.

Brune, D. C., P. D. Gerola, and J. M. Olson. 1990. Circular dichroism of green bacterial chlorosomes. *Photosynth. Res.* 24:253–263.

Causgrove, T. P., D. C. Brune, J. Wang, B. P. Wittmershaus, and R. E. Blankenship. 1990. Energy transfer kinetics in whole cells and isolated chlorosomes of green photosynthetic bacteria. *Photosynth. Res.* 26: 39–48.

Chiefari, J., K. Griebenow, F. Fages, N. Griebenow, T. S. Balaban, A. R. Holzwarth, and K. Schaffner. 1995. Models for the pigment organization in the chlorosomes of photosynthetic bacteria: diastereoselective control of in vivo Bacteriochlorophyll *c*-s aggregation. *J. Phys. Chem.* 99: 1357–1365.

de Boer, S., K. J. Vink, and D. A. Wiersma. 1987. Optical dynamics of condensed molecular aggregates: an accumulated photon echo and hole-burning study of the J-aggregate. *Chem. Phys. Lett.* 137:99–106.

Fetisova, Z., and K. Mauring. 1992. Experimental evidence of oligomeric organization of antenna bacteriochlorophyll *c* in green bacterium *Chloroflexus aurantiacus* by spectral hole burning. *FEBS Lett.* 307:371–374.

Fetisova, Z., and K. Mauring. 1993. Spectral hole burning stud of intact cells of green bacterium *Chlorobium limicola. FEBS Lett.* 323:159–162.

Fetisova, Z., A. Freiberg, K. Mauring, V. Novoderezhkin, A. Taisova, and K. Timpmann. 1996. Excitation energy transfer in chlorosomes of green bacteria: theoretical and experimental studies. *Biophys. J.* 71:995–1010.

Fidder, H., J. Knoester, and D. A. Wiersma. 1991. Optical properties of disordered molecular aggregates: a numerical study. *J. Chem. Phys.* 95:7880–7890.

Fletcher, R. 1980. Practical Methods of Optimization, vol. 1: Unconstrained optimization. John Wiley and Sons, New York.

Frese, R., U. Oberheide, I. H. M. van Stokkum, R. van Grondelle, M. Foidl, J. Oelze, and H. van Amerongen. 1997. The organization of bacteriochlorophyll *c* in chlorosomes from *Chloroflexus aurantiacus* and the structural role of carotenoids and protein: an absorption, linear dichroism, circular dichroism and Stark spectroscopy study. *Photosynth. Res.* 54:115–126.

Griebenow, K., and A. R. Holzwarth. 1989. Pigment organization and energy transfer in green bacteria. 1. Isolation of native chlorosomes free of bound bacteriochlorophyll *a* from *Chloroflexus aurantiacus* by gel-electrophoretic filtration (GEF). *Biochim. Biophys. Acta.* 973:235–240.

Griebenow, K., M. G. Müller, and A. R. Holzwarth. 1990. Picosecond energy transfer kinetics between different pigment pools in chlorosomes from the green bacterium *Chloroflexus aurantiacus. In* Molecular Biology of Membrane-Bound Complexes in Phototrophic Bacteria. G. Drews and E. A. Dawes, editors. Plenum Press, New York. 383–387.

Griebenow, K., A. R. Holzwarth, F. van Mourik, and R. van Grondelle. 1991. Pigment organization and energy transfer in green bacteria. 2. Circular and linear dichroism spectra of protein-containing and protein-free chlorosomes isolated from *Chloroflexus aurantiacus* strain OK-70-fl*. *Biochim. Biophys. Acta.* 1058:194–202.

Hildebrandt, P., K. Griebenow, A. R. Holzwarth, and K. Schaffner. 1991. Resonance Raman spectroscopic evidence for the identity of the bacteriochlorophyll *c* organization in protein-free and protein-containing chlorosomes from *Chloroflexus aurantiacus. Z. Naturforsch.* 46C: 228–232.

Hildebrandt, P., H. Tamiaki, A. R. Holzwarth, and K. Schaffner. 1994. Resonance Raman spectroscopic study of metallochlorin aggregates. Implications for the supramolecular structure of chlorosomal BChl *c* antennae of green bacteria. *J. Phys. Chem.* 98:2192–2197.

Hirota, M., T. Moriyama, K. Shimada, M. Miller, J. M. Olson, and K. Matsuura. 1992. High degree of organization of bacteriochlorophyll c in chlorosome-like aggregates spontaneously assembled in aqueous solution. *Biochim. Biophys. Acta.* 1099:271–274.

Holzwarth, A. R., K. Griebenow, and K. Schaffner. 1990a. A photosynthetic antenna system which contains a protein-free chromophore aggregate. *Z. Naturforsch.* 45C:203–206.

Holzwarth, A. R., M. G. Müller, and K. Griebenow. 1990b. A photosynthetic antenna system which contains a protein-free chromophore aggregate. *Z. Naturforsch.* 45c:203–206.

Holzwarth, A. R., K. Griebenow, and K. Schaffner. 1992. Chlorosomes, photosynthetic antennae with novel selforganized pigment structures. *J. Photochem. Photobiol. A.* 65:61–71.

Holzwarth, A. R., and K. Schaffner. 1994. On the structure of bacteriochlorophyll molecular aggregates in the chlorosomes of green bacteria: a molecular modelling study. *Photosynth. Res.* 41:225–233.

Houssier, C., and K. Sauer. 1970. Circular dichroism and magnetic circular dichroism of the chlorophyll and protochlorophyll pigments. *J. Am. Chem. Soc.* 92:779–791.

Iversen, J. J. L., M. Nielsen, and R. P. Cox. 1989. Design and performance of a simple, inexpensive, modular labaratory-scale bioreactor. *Biotechnol. Edu:* 1:11–15.

James, D. R., and W. R. Ware. 1986. Recovery of underlying distributions of lifetimes from fluorescence decay data. *Chem. Phys. Lett.* 126:7–11.

Joo, Taiha, and A. C. Albrecht. 1993. Electron dephasing studies of molecules in solution at room temperature by femtosecond degenerate four wave mixing. *Chem. Phys.* 176:233–247.

Keller, D., and C. Bustamante. 1986. Theory of the interaction of light with large inhomogeneous molecular aggregates. II. Psi-type circular dichroism. *J. Chem. Phys.* 84:2972–2980.

Landl, G., T. Langthaler, H. W. Engl, and H. F. Kauffmann. 1991. Distribution of event times in time-resolved fluorescence: the exponential series approach—algorithm, regularization, analysis. *J. Comput. Phys.* 95:1–28.

Lehmann, R. P., R. A. Brunisholz, and H. Zuber. 1994. Giant circular dichroism of chlorosomes from *Chloroflexus aurantiacus* treated with 1-hexanol and proteolytic enzymes. *Photosynth. Res.* 41:165–173.

Ma, Y-Z., F. Feldchtein, A. I. Korytin, A. M. Kiselev, M. Miller, and T. Gillbro. 1996a. Ultrafast energy transfer kinetics in chlorosomes from *Chloroflexus aurantiacus. Brazilian J. Phys.* 26:530–542.

Ma, Y-Z., R. P. Cox, T. Gillbro, and M. Miller. 1996b. Bacteriochlorophyll organization and energy transfer kinetics in chlorosomes from *Chloroflexus aurantiacus* depend on the light regime during growth. *Photosynth. Res.* 47:157–165.

Mizoguchi, T., L. Limantara, K. Matsuura, K. Shimada, and Y. Koyama. 1996. Aggregation forms of 8-ethyl farnesyl bacteriochlorophyll *c* in methanol-chloroform mixtures as revealed by 1H NMR spectroscopy. *J. Mol. Struct.* 379:249–265.

Mizoguchi, T., S. Sakamoto, Y. Koyama, K. Ogura, and F. Inagaki. 1998. The structure of the aggregate form of bacteriochlorophyll *c* showing the Q_y absorption above 740 nm as determined by the ring-current effects on ^1H and ^{13}C nuclei and by ^1H-^1H intermolecular NOE correlations. *Photochem. Photobiol.* 67:239–248.

Mukamel, S. 1995. Principles of Nonlinear Optical Spectroscopy. Oxford University Press, New York.

Müller, M. G., K. Griebenow, and A. R. Holzwarth. 1990. Fluorescence lifetime measurements of energy transfer in chlorosomes and living cells of *Chloroflexus aurantiacus* OK-70fl. *In* Current Research of Photosynthesis. II. M. Baltscheffsky, editor. Kluwer Academic Publishers, Dordrecht. 177–180.

Müller, M. G., K. Griebenow, and A. R. Holzwarth. 1993. Picosecond energy transfer and trapping kinetics in living cells of the green bacterium *Chloroflexus aurantiacus. Biochim. Biophys. Acta.* 1144:161–169.

Novoderezhkin, V. I., and Z. G. Fetisova. 1996. Structure of bacteriochlorophyll aggregates in chlorosomes of green bacteria: a spectral hole burning study. *Biochem. Mol. Biol. Int.* 40:243–252.

Nozawa, T., K. Ohtomo, M. Suzuki, H. Nakagawa, Y. Shikama, H. Konami, and Z-Y. Wang. 1994. Structures of chlorosomes and aggregated Bchl *c* in *Chlorobium tepidum* from solid state high resolution CP/MAS ^{13}C NMR. *Photosynth. Res.* 41:211–223.

Olson, J. M., P. D. Gerola, G. H. van Brakel, R. F. Meiburg, and H. Vasmel. 1985. Bacteriochlorophyll a- and c-protein complexes from chlorosomes of green sulfur bacteria compared with bacteriochlorophyll *c* aggregates in CH2Cl2-hexane. *In* Antennas and Reaction Centers of Photosynthetic Bacteria, Springer Ser. Chem. Phys. Vol. 42. M. E. Michel-Beyerle, editor. Springer, Berlin. 67–73.

Olson, J. M., D. C. Brune, and P. D. Gerola. 1990. Organization of chlorophyll and protein in chlorosomes. *In* Molecular Biology of Membrane-Bound Complexes in Phototrophic Bacteria. G. Drews and E. A. Dawes, editors. Plenum Press, New York. 227–234.

Olson, J. M. 1998. Chlorophyll organization and function in green photosynthetic bacteria. *Photochem. Photobiol.* 67:61–75.

Oelze, J. 1985. Analysis of bacteriochlorophylls. *Methods Microbiol.* 18: 257–284.

Pearlstein, R. M. 1991. Theoretical interpretation of antenna spectra. *In* Chlorophylls. H. Scheer, editor. CRC Press, London. 1047–1078.

Prokhorenko, V. I., M. V. Melishchuk, and E. A. Tikhonov. 1983. Pump-probe measurements of ultrafast relaxation in dyes. *Reprint No. 1, Inst. Phys. Urk. Acad. Sci.* 1–32.

Psencik, J., M. Vacha, F. Adamec, M. Ambroz, J. Dian, J. Bocek, and J. Hala. 1994. Hole burning study of excited state structure and energy transfer dynamics of bacteriochlorophyll *c* in chlorosomes of green sulphur photosynthetic bacteria. *Photosynth. Res.* 42:1–8.

Psencik, J., T. Polivka, P. Nemec, J. Dian, J. Kundra, P. Maly, and J. Hala. 1998. Fast energy transfer and exciton dynamics in chlorosomes of the green sulphur bacterium *Chlorobium tepidum. J. Phys. Chem.* 102: 4392–4398.

Savikhin, S., Y. Zhu, S. Lin, R. E. Blankenship, and W. S. Struve. 1994. Femtosecond spectroscopy of chlorosome antennas from the green photosynthetic bacterium *Chloroflexus aurantiacus. J. Phys. Chem.* 98: 10322–10334.

Savikhin, S., P. I. van Noort, Y. Zhu, S. Lin, R. E. Blankenship, and W. S. Struve. 1995a. Ultrafast energy transfer in light-harvesting chlorosomes from the green sulphur bacterium *Chlorobium tepidum. Chem. Phys.* 194:245–258.

Savikhin, S., P. I. van Noort, R. E. Blankenship, and W. S. Struve. 1995b. Femtosecond probe of structural analogies between chlorosomes and bacteriochlorophyll *c* aggregates. *Biophys. J.* 69:1100–1104.

Savikhin, S., Y. Zhu, R. E. Blankenship, and W. S. Struve. 1996a. Intraband energy transfer in the Bchl *c* antenna of chlorosomes from the green photosynthetic bacterium *Chloroflexus aurantiacus. J. Phys. Chem.* 100:17978–17980.

Savikhin, S., Y. Zhu, R. E. Blankenship, and W. S. Struve. 1996b. Ultrafast energy transfer in chlorosomes from the green photosynthetic bacterium *Chloroflexus aurantiacus. J. Phys. Chem.* 100:3320–3322.

Savikhin, S., D. R. Buck, W. S. Struve, R. E. Blankenship, A. S. Taisova, V. I. Novoderezhkin, and Z. G. Fetisova. 1998. Excitation delocalization in the bacteriochlorophyll *c* antenna of the green bacterium *Chloroflexus aurantiacus* as revealed by ultrafast pump-probe spectroscopy. *FEBS Lett.* 430:323–326.

Schaffner, K., and A. R. Holzwarth. 1997. Selbstorganisation von Biomolekülen am Beispiel von Bacteriochlorophyllen in natürlichen Antennensystemen—ein Weg für die Entwicklung photoaktiver supramolekularer Funktionssysteme. *Leopoldina.* 42:205–220.

Siemiarczuk, A., B. D. Wagner, and W. R. Ware. 1990. Comparison of the maximum entropy and exponential series methods for the recovery of distributions of lifetimes from fluorescence lifetime data. *J. Phys. Chem.* 94:1661–1666.

Shen, Y. R. 1984. The principles of nonlinear optics. Wiley-Interscience Publication, New York.

Staehelin, L. A., J. R. Golecki, R. C. Fuller, and G. Drews. 1978. Visualization of supramolecular architecture of chlorosomes (*Chlorobium* type vesicles) in freeze-fractured cells of *Chloroflexus aurantiacus. Arch. Microbiol.* 119:269–277.

Staehelin, L. A., J. R. Golecki, and G. Drews. 1980. Supramolecular organization of chlorosomes (*Chlorobium* vesicles) and of their membrane attachment sites in *Chlorobium limicola. Biochim. Biophys. Acta.* 589:30–45.

Stanier, R. Y., and J. H. C. Smith. 1960. The chlorophylls of green bacteria. *Biochem. Biophys. Acta.* 41:478–484.

Steensgaard, D. B., K. Matsuura, R. P. Cox, and M. Miller. 1997. Changes in bacteriochlorophyll *c* organization during acid treatment of chlorosomes from *Chlorobium tepidum. Photochem. Photobiol.* 65:129–134.

Steensgaard, D. B., C. A. van Walree, H. Permentier, L. Baneras, C. M. Borrego, J. Garcia-Gil, T. J. Aartsma, J. Amesz, and A. R. Holzwarth. 2000. Fast energy transfer between BChl *d* and BChl *c* in chlorosomes of the green sulfur bacterium *Chlorobium limicola. Biochim. Biophys. Acta.* 1457:71–80.

Tamiaki, H., M. Amakawa, Y. Shimono, R. Tanikaga, A. R. Holzwarth, and K. Schaffner. 1996. Synthetic zinc and magnesium chlorin aggregates as models for supramolecular antenna complexes in chlorosomes of green photosynthetic bacteria. *Photochem. Photobiol.* 63:92–99.

van Rossum, B.-J., G. J. Boender, F. M. Mulder, J. Raap, T. S. Balaban, A. R. Holzwarth, K. Schaffner, S. Prytulla, H. Oschkinat, and H. J. M. de Groot. 1998a. Multidimensional CP-MAS 13C NMR of uniformy enriched chlorophyll. *Spectrochim. Acta.* A54:1167–1176.

van Rossum, B.-J., B. Y. van Duyl, D. B. Steensgaard, T. S. Balaban, A. R. Holzwarth, K. Schaffner, and H. J. M. de Groot. 1998b. Evidence from solid state NMR correlation spectroscopy for two interstack arrangements in the chlorosome antenna system. *In* Photosynthesis: Mechanism and Effects, vol. 1: Proceedings of XI International Congress on Photosynthesis, Budapest. G. Garab, editor. Kluwer Academic Publishers, Dordrecht. 117–120.

van Rossum, B., C. Soede, D. Steensgaard, A. R. Holzwarth, K. Schaffner, J. Raap, J. Lugtenburg, P. Gast, A. Hoff, and H. de Groot. 1999. Magic angle spinning NMR of photosynthetic components. Proceedings of VIIIth European Conference on the Spectroscopy of Biological Molecules, Twente, The Netherlands. (In press.)

van Walree, C. A., Y. Sakuragi, D. B. Steensgaard, C. S. Bösinger, N-U. Frigaard, R. P. Cox, A. R. Holzwarth, and M. Miller. 1999. Effect of alkaline treatment on bacteriochlorophyll *a*, quinones, and energy transfer in chlorosomes from *Chlorobium tepidum* and *Chlorobium phaeobacteroides. Photochem. Photobiol.* 69:322–328.

van Burgel, M., D. A. Wiersma, and K. Duppen. 1995. The dynamics of one-dimensional excitons in liquids. *J. Chem. Phys.* 102:20–33.

Wahlund, T. M., C. R. Woese, R. W. Castenholz, and M. T. Madigan. 1991. A thermophilic green sulfur bacterium from New Zealand hot springs, *Clorobium tepidum* sp. nov. *Arch. Microbiol.* 156:81–90.

Wang, Z-Y., G. Marx, M. Umetsu, M. Kobayashi, M. Mimuro, and T. Nozawa. 1995. Morphology and spectroscopy of chlorosomes from *Chlorobium tepidum* by alcohol treatments. *Biochim. Biophys. Acta.* 1232:187–196.